LARGE EDDY SIMULATION OF TURBULENT BOUNDARY-LAYER SEPARATION

Stefan Hickel & **Nikolaus A. Adams**

Institute of Aerodynamics, Technische Universität München, D-85747 Garching, Germany.
E-mail: sh@tum.de

ABSTRACT

Highly resolved Large Eddy Simulation (LES) of turbulent boundary-layer separation are conducted. The behavior of incompressible fully-turbulent flat-plate boundary-layer flow subjected to a constant adverse pressure gradient (APG) is investigated. Reynolds number and pressure-gradient parameters are adapted to measurements conducted by Indinger *et al.* in a closed-circuit water tunnel. A special focus of analysis is placed on scaling laws for the mean-velocity profiles under non-equilibrium conditions approaching pressure-induced separation. Our computational results suggest that classical inner scaling remains valid for non-equilibrium even with intermittent detachment. Best predictions for the outer region are obtained with the scaling of Zaragola and Smits.

INTRODUCTION

There has been considerable controversy regarding the behavior of the mean-velocity profile of turbulent boundary layers approaching separation (George, 2006; Indinger et al., 2006; Maciel et al., 2006). Asymptotic expansions predict independence from the pressure gradient for the inner region, provided the Reynolds number is large (Panton, 2005). While some experiments (Ludwieg and Tillmann, 1949; Skåre and Krogstad, 1994, e.g.) show that the classical logarithmic law is valid even under a strong adverse pressure gradient (APG) and non-equilibrium conditions, other experiments indicate that, based on inner scaling, the mean velocity profile is not self-similar when approaching separation (Dengel and Fernholz, 1990; Nagano et al., 1998, e.g.).

Recently, Indinger et al. (2006, 2004) have presented measurements for a fully turbulent flat-plate boundary layer with a constant APG, for a detailed description refer to Indinger (2005). Fig. 1 shows the experimental setup in the test section of a closed-circuit water tunnel with flow from left to right. The measurements were conducted in the boundary layer developing on an inclined flat plate. A flexible curved wall on the opposite side is employed to impose the pressure gradient to the flow, where the pressure-gradient parameters can be controlled by adjusting the curvature. The test section has a cross section of 0.4×0.4 square meters and an overall length of 0.8 meters. The flat plate, inclined by 4 degrees, has an overall length of 0.725 meters and a flap to prevent trailing-edge separation. The plate surface is made from mirrored borosilicate glass which facilitates measurements close to the wall. Several auxiliary devices that are necessary to control the flow quality. A bypass system below the flat plate and a suction system have been installed to control the stagnation point flow at the elliptic leading edge of the plate. To prevent separation of the boundary layer on the opposite wall due to curvature effects, a second suction system consisting of three slots is installed at the upper rear end of the test section.

In the spanwise-centered plane, streamwise velocity profiles were measured using a LASER Doppler anemometry (LDA) system. For measurements of the wall shear stress, a Preston tube was used. These measurements cannot provide fully-3D statistics of the turbulent non-equilibrium flow. To gain a deeper understanding of the behavior in the vicinity of the pressure-induced separation a numerical investigation by Large Eddy Simulation (LES) was carried out which is reported in the following.

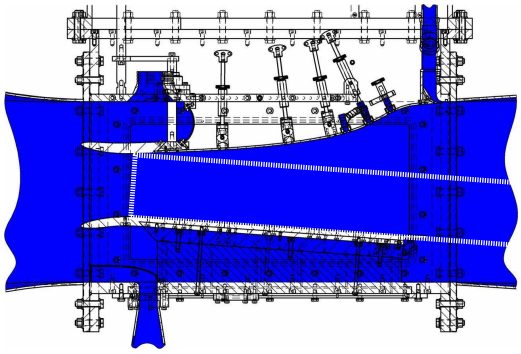

Figure 1: Experimental setup in the test section of a water tunnel. The computational domain of the present LES is marked by the dashed white line.

It should be noted that under the considered conditions the APG leads to massive separation with a thickness of about $2\delta^*$ in terms of the attached boundary layer thickness. The pressure-gradient induced separation is highly unsteady. In our LES, the instantaneous separation line has excursions which are significantly larger than the mean boundary-layer thickness of the incoming flow.

NUMERICAL METHOD

Implicit-LES methodology and subgrid-scale modeling

Further development of LES faces as major obstacle the strong coupling between subgrid-scale (SGS) model and the truncation error of the numerical discretization. SGS models for LES generally operate on a range of scales which is marginally resolved by the underlying discretization scheme. One can exploit this link by developing discretization methods where the truncation error itself functions as implicit SGS model. Approaches where SGS model and numerical discretization are merged are called implicit LES. Many approaches to implicit LES can be taken, a comprehensive review is given in the book of Grinstein et al. (2007). Mostly, given nonlinearly stable discretization schemes for the convective

fluxes are used as main element of implicit SGS models. A numerical analysis of Garnier et al. (1999), however, comes to the conclusion that the application of off-the-shelf upwind, variation-limited, or non-oscillatory schemes is not recommendable.

Using implicit LES for prediction requires discretization schemes which are specially designed, optimized, and validated for the differential equation to be solved. In order to avoid that suitable schemes have to be found merely by conjecture, we have recently developed a systematic framework for ILES based on deconvolution methods (Adams et al., 2004; Hickel et al., 2006). The resulting so-called *Adaptive Local Deconvolution Method* (ALDM) represents a full merging of numerical discretization and subgrid-scale model.

Optimal model parameters of ALDM are determined by minimizing a cost function which measures the difference between spectral numerical viscosity and the eddy viscosity from EDQNM theory for isotropic turbulence (Hickel et al., 2006). With these parameters, the spectral eddy viscosity of the ALDM scheme exhibits a low-wavenumber plateau at the correct level and reproduces the typical cusp shape up to the cut-off wave number at the correct magnitude when applied to canonical inertial-range turbulence. Recently, this analysis has been extended to the passive-scalar transport equation (Hickel et al., 2006).

ALDM has been established as a reliable, accurate, and efficient method for LES. Predictions of ALDM agree well with theory and experimental data. Various applications, e.g. to three-dimensional homogeneous isotropic turbulence (Hickel et al., 2006), to plane channel flow (Hickel et al., 2005), and to the separated flow in a channel with periodic restrictions (Hickel et al., 2006), demonstrate the good performance of the implicit model. It has been shown that the implicit SGS model performs at least as well as established explicit models. This is attributed to the fact that physical SGS modeling approaches are incorporated into the design of the discretization scheme, and that discretization effects are fully taken into account within the SGS model formulation.

Implementation

The incompressible Navier-Stokes equations are discretized on a staggered Cartesian mesh. For time advancement an explicit third-order Runge-Kutta scheme with coefficients as proposed by Shu (1988) is used. We use a Courant-Friedrichs-Lewy limit of CFL = 1.0 for all simulations. All results presented in this paper are obtained by the simplified adaptive local deconvolution method (Hickel and Adams, 2006) that represents a computationally more efficient implementation of the original ALDM. The pressure-Poisson equation and diffusive terms are discretized by second-order centered differences. The Poisson solver employs fast Fourier transforms in the spanwise direction and the stabilized bi-conjugate gradient method in the streamwise and wall-normal directions. The Poisson equation is solved at every Runge-Kutta substep.

Computational grid and boundary conditions

The computational domain considered in the LES, as indicated by a dashed white line in Fig. 1, represents only a part of the experimental setup. The flow within this domain is determined by the surrounding flow which has to be modeled by imposing appropriate boundary conditions.

The computational domain of the LES has an overall length of 1.01 meters and is discretized by $2038 \times 144 \times 144$ finite volumes. The spanwise and wall-normal extents are 0.036 meters and 0.15 meters, respectively. For comparison, the inflow boundary layer thickness is $\delta^*(x = 0) = 0.0008$ meters. The grid spacing is homogeneous in streamwise and in spanwise directions. In wall-normal direction a hyperbolic stretching is used to increase resolution near the wall. At the domain boundaries three layers of ghost cells are added so that stencils reaching beyond the domain boundary can be used. The employed methods for filling these ghost cells are described below.

Spanwise periodicity was imposed since the flow is supposed to be homogeneous in this direction. At the surface of the flat plate a no-slip condition is imposed. The boundary layer is resolved and no wall model is used. The ghost cells are filled with the analytical solution for Stokes flow as recommended by Morinishi et al. (1998).

The free-stream interface is modeled by prescribing pressure $p = p_{fs}$ and face-normal derivatives of the mean velocity $\partial_y \langle \boldsymbol{u} \rangle = \boldsymbol{0}$, and by solving for velocity fluctuations $\partial_y \boldsymbol{u}' = -\alpha \boldsymbol{u}'$ with $\alpha = 1/(4\Delta_y)$. The latter results in the decay condition $\boldsymbol{u}'(y) \propto \exp(-\alpha y)$. The value of the parameter α was determined from the wavelength of numerically induced oscillations that were observed when the decay condition was not used. Ghost cells are filled by solving a discrete second-order approximation of the above equations.

At the inlet, fully turbulent inflow data are generated using a recycling technique, similar to that of Lund et al. (1998): Instantaneous turbulent structures are extracted at a downstream distance $l_{rec} \approx 10\delta$. Inside the boundary layer, target profiles for the fluctuating velocities are taken from Spalart's zero-pressure-gradient boundary-layer DNS (Spalart, 1988) at $\mathrm{Re}_\theta = 670$. In the outer flow region, isotropic turbulence is assumed with a turbulence level of $Tu = 0.03$ matched to the water-tunnel experiment. Recycling techniques can sustain spurious oscillations with a wavelength proportional to the recycling length. In order to damp these oscillations the re-scaling factors are computed for each ghost-cell plane separately: For the innermost ghost-cell plane, target profiles are taken from the DNS of Spalart (1988). For the remaining two upstream planes, the target fluctuation profiles are damped such that $\partial_x \langle \boldsymbol{u}' \rangle = \langle \boldsymbol{u}' \rangle / l_{rec}$ is satisfied.

At the outlet, the ghost cells are filled by extrapolation in such a way that $\partial_x p = 0$ and $\partial_x^2 \boldsymbol{u} = \boldsymbol{0}$ are fulfilled for a second-order centered discretization. No artificial damping or sponge zone is used.

RESULTS AND DISCUSSION

General overview

A first impression of the investigated flow can be obtained from mean profiles of streamwise and wall-normal velocity components that are shown for the entire computational domain in Fig. 2. The influence of a strong adverse pressure gradient is evident. The mean-flow deceleration results in an increasing fraction of back-flow events and eventually causes strong boundary-layer separation. The boundary-layer separation is accompanied by a strong wall-normal velocity component and intense interactions with the outer flow. The shape of the separation bubble is indicated by two lines that represent

different criteria: The locations where the mean streamwise velocity component does vanish $\langle u \rangle = 0$ and the locations where forward flow and upstream flow have equal probability ($\chi = 0.5$). Both criteria give a similar impression, however, notable differences are observed close to the separation point.

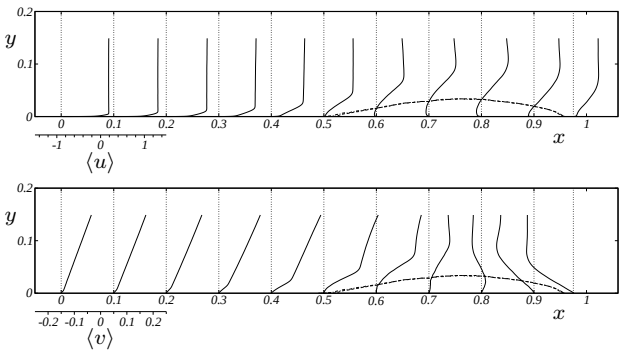

Figure 2: Mean velocity profiles for present LES of an APG turbulent boundary layer. ——— mean velocity, – – – – $\langle u \rangle = 0$, ·—·—·— $\chi = 0.5$.

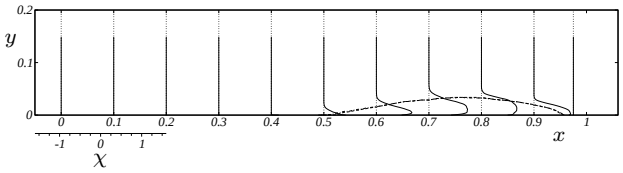

Figure 3: Reverse flow parameter for present LES of an APG turbulent boundary layer.

The probability of back flow is measured by the reverse-flow parameter

$$\chi = \frac{1}{2} - \frac{1}{2} \left\langle \frac{u}{|u|} \right\rangle , \qquad (1)$$

where χ denotes the fraction of time that the flow moves upstream. Wall-normal profiles of the value of χ are shown in Fig. 3 and streamwise profiles are shown in Fig. 4. We observe that flow separation is accompanied by the shift of the location of maximum χ away from the wall towards the detached shear layer.

The following terminology has been proposed by Simpson (1981, 1989) to define the separation state quantitatively: *Incipient detachment* (ID) occurs with $\chi = 0.01$, *intermittent transitory detachment* (ITD) occurs with $\chi = 0.2$, *transitory detachment* (TD) occurs with $\chi = 0.5$, and *detachment* (D) occurs where the time-averaged wall shearing stress is zero. The corresponding locations for the LES of the present configuration are given in Tab. 1. As most available data, our computational results confirm that TD and D occur at the same location.

The mean static pressure imposed as a boundary condition at the free-stream interface is shown in Fig. 4b. The mean pressure distribution at the wall, see Fig. 4b, is the nonlinear response of the flow and strongly influenced by the boundary-layer separation. The oscillatory motion of detached flow zones have a significant effect on the upstream flow that results in substantial deviation of the wall pressure from the imposed free-stream condition. In the experiments, the pressure has been measured at the plate surface only. Hence, the free-stream pressure boundary condition for the present LES had to be reconstructed by a large number of low-resolution trials to obtain best possible agreement of the wall-pressure distribution with the experimental data.

Table 1: Separation state near the wall for present LES in Simpson's terminology (Simpson, 1981).

Term	Definition	Location
ID	$\chi = 0.01$	$x = 0.287$
ITD	$\chi = 0.2$	$x = 0.457$
TD	$\chi = 0.5$	$x = 0.489$
D	$\langle \tau_w \rangle = 0$	$x = 0.490$

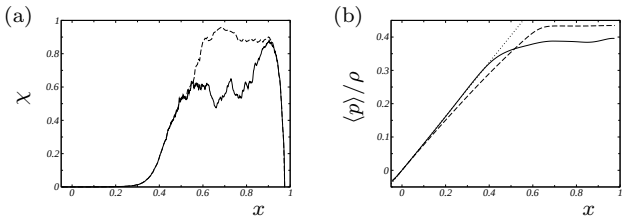

Figure 4: (a) Reverse-flow parameter: ——— at the wall and – – – – maximum value. (b) Mean static pressure at the – – – – free-stream interface and at the ——— wall. The ····· dotted line denotes the target pressure gradient of 810 Pa/m according to experimental reference data.

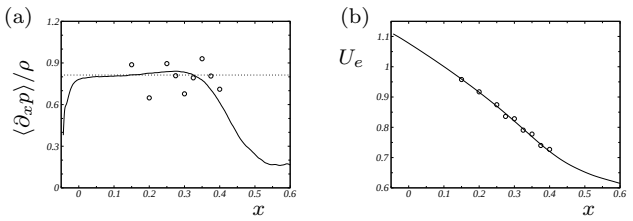

Figure 5: (a) Mean pressure gradient at the wall, and (b) free-stream velocity at the boundary-layer edge for ∘ experiment and ——— LES.

Cross-validation of numerical and experimental results

The resulting wall-pressure gradients for LES and the experiment are shown in Fig. 5a. Despite the the usual noise in derivatives computed from experimental data, LES results and experiment agree well. This first impression is confirmed by the observed deceleration of the free-steam velocity U_e , see Fig. 5b, that can be measured more accurately. Mean-flow deceleration is directly caused by the APG through Bernoulli's equation and the excellent agreement of U_e confirms that both the pressure gradient and the curvature of streamlines are reproduced correctly.

The relevant velocity scale for flow in the near-wall region within the boundary layer is the wall-friction velocity $U_\tau = \sqrt{\nu |\langle \partial_y u \rangle|_{wall}}$. Fig. 6a shows the wall-friction velocity from Indinger (2005) and for the present LES. The graph indicates differences between LES and experiment that become more pronounced in the local non-dimensional wall-friction coefficient $C_f = 2U_\tau^2/U_\delta^2$, see Fig. 6b. We believe that these differences mostly result from errors in the experimental determination of U_τ (Indinger, personal communication).

Indinger et al. (2006) used a Preston tube to measure the

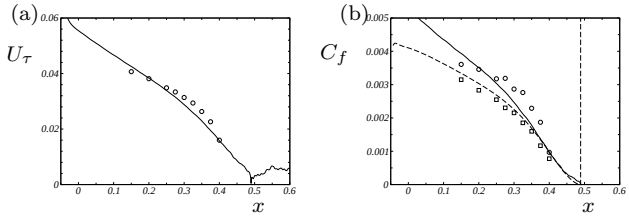

Figure 6: (a) Wall-friction velocity U_τ ——— present LES, ∘ Preston-tube measurement. (b) Local wall-friction parameter C_f ——— from present LES, ∘ Preston-tube measurement, – – – – correlation of Fernholtz (1964) using LES data, □ correlation of Fernholtz (1964) using LDA measurements.

dynamic pressure at the wall. The wall-friction velocity U_τ has been computed by means of tabulated calibration data of Head and Ram (1971). By construction, Preston-tube measurements are erroneous in flow regions with instantaneous backflow, i.e. from ID onwards. The applicability of this method to attached flow is questionable in case of strong pressure gradient (Patel, 1965). Our claim is corroborated by an empirical correlation for C_f. Following Fernholtz (1964),

$$C_f = 0.058\mathrm{lg}(8.05/H_{12}^{1.818})^{1.705}\mathrm{Re}_\theta^{-0.268} \tag{2}$$

allows to approximate the local wall-friction coefficient by a functional of non-dimensional integral parameters, that can be measured rather accurately. In Fig. 6b this correlation is applied to both experimental and numerical data. A good agreement of simulation and experiment is observed. In the region with significant backflow, between ID and D, the correlation functional of Fernholtz (1964) gives C_f almost identical to that computed from the wall-friction of the LES.

A turbulent boundary layer can by characterized by several length scales. The boundary-layer thickness δ serves as a measure for the largest structures in the boundary-layer flow. δ is defined as the distance from the wall where 99 percent (δ_{99}) of the free-stream velocity U_e is reached. In APG boundary layer flow, however, the velocity is not constant in the free stream. For the experimental data, the LDA measurement points representing the transition between boundary layer and free stream were chosen by Indinger (2005) manually. For the LES data, the boundary layer edge is determined as the point where the streamwise velocity starts to diverge from the linear dependency, which is valid for the external flow, with decreasing wall distance. The velocity at this point is defined as U_e and δ follows from $\delta = y|_{\langle u\rangle = U_\delta}$ with $U_\delta = 0.99U_e$. The viscous length scale $l^+ = \nu/U_\tau$ is used to characterize the size of the smallest coherent structures that occur close to the wall. Graphs for both length scales are shown in Fig. 7. The viscous length scale l^+ is computed from its definition $l^+ = \nu/U_\tau$ using the wall-friction velocity U_τ that has been discussed already. Differences between LES and experiment result from the Preston-tube measurement of U_τ.

Because of such uncertainties, length scales based on integral definitions are more robust than δ and l^+. Fig. 8 shows the boundary-layer displacement thickness

$$\delta^* = \int_0^\infty \left(1 - \frac{\langle u\rangle}{U_\delta}\right) dy, \tag{3}$$

and the boundary-layer momentum-loss thickness

$$\delta_\theta = \int_0^\infty \frac{\langle u\rangle}{U_\delta}\left(1 - \frac{\langle u\rangle}{U_\delta}\right) dy. \tag{4}$$

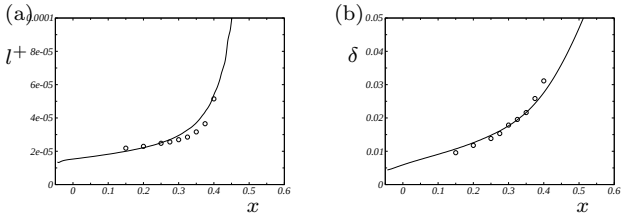

Figure 7: (a) viscous length-scale for: ——— present LES and ∘ Preston-tube measurement, (b) boundary-layer thickness for: ——— present LES and ∘ LDA measurement.

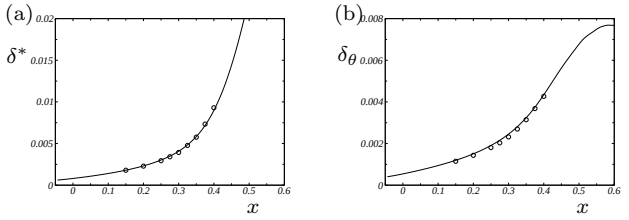

Figure 8: Integral measures for the boundary-layer thickness: (a) displacement thickness, (b) momentum thickness. ——— present LES , ∘ LDA measurement.

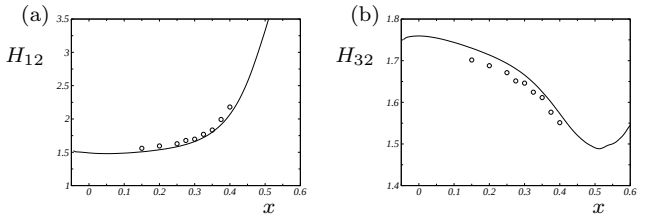

Figure 9: Shape parameters: (a) H_{12} displacement thickness to momentum-loss thickness, (b) H_{32} energy-loss thickness to momentum-loss thickness. ——— present LES , ∘ LDA measurement.

Pressure gradient and incipient separation result in a fast growth of the boundary-layer thicknesses. We observe a good agreement between experiment and simulation for δ^* and δ_θ.

The different thickness measures are frequently used to define non-dimensional parameters characterizing the shape of the mean velocity profile. Fig. 9 show the shape parameters H_{12} and H_{32} which are defined as the ratio of displacement thickness to momentum thickness, and as the ratio of energy thickness to momentum thickness, respectively. At the inflow, H_{12} is almost constant at a level of 1.5. The parameter H_{12} increases with incipient backflow and doubles its value before boundary-layer separation. H_{23} shows a notable inflow transient, that might result from the fact that zero-pressure-gradient (ZPG) velocity profiles and statistics were imposed at the inflow. After this transient, H_{23} decreases from about 1.75 to a minimum of about 1.5 at detachment. Simulation and experiment show identical qualitative behavior, however, LES predicts slightly higher values for H_{32} and slightly lower values for H_{12} than determined experimentally. Fig. 10 shows Reynolds numbers Re_{δ^*} and $\mathrm{Re}_{\delta_\theta}$ based on displacement thickness and momentum thickness, respectively, for experiment and computation.

Numerous dimensionless pressure-gradient parameters have been proposed in order to classify and to compare APG boundary-layer flows. Fig. 11 shows four widely used param-

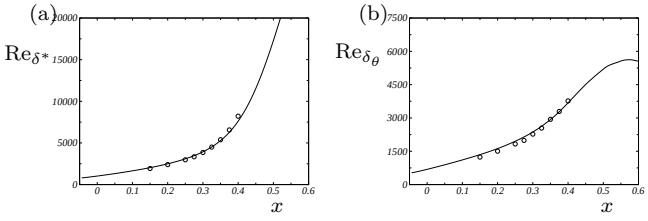

Figure 10: Reynolds numbers: (a) Reynolds number based on displacement thickness, (b) Reynolds number based on momentum-loss thickness, ——— present LES , ∘ LDA measurement.

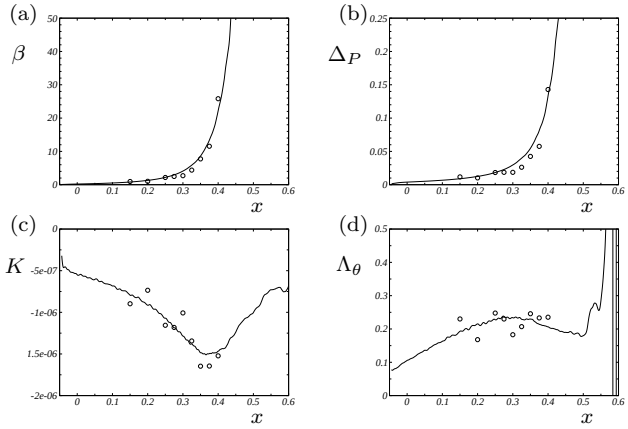

Figure 11: Pressure-gradient parameters (a) Clauser pressure-gradient parameter, (b) Patel pressure gradient, (c) dimensionless pressure-gradient parameter K, (d) dimensionless pressure-gradient parameter Λ_θ.

eters, namely the Clauser pressure parameter

$$\beta = \frac{\delta^*}{\rho U_\tau^2} \langle \partial_x p \rangle \,, \tag{5}$$

the Patel pressure gradient

$$\Delta_P = \frac{\nu}{\rho U_\tau^3} \langle \partial_x p \rangle \,, \tag{6}$$

the pressure-gradient parameter

$$\Lambda_\theta = \frac{\delta_\theta}{\rho U_\delta^2 \partial_x \delta_\theta} \langle \partial_x p \rangle \,, \tag{7}$$

and the pressure-gradient parameter

$$K = \frac{\nu}{U_\delta^2} \langle \partial_x U_\delta \rangle \,. \tag{8}$$

The latter parameter has the advantage that it does not incorporate pressure gradient and wall-shear stress. For all pressure-gradient parameters LES results and experimental data agree reasonably well.

Scaling of mean velocity profiles

A special focus has been on the scaling of the mean velocity profile under non-equilibrium conditions in the vicinity of pressure-induced separation. Present LES and experimental results show consistently that the mean velocity profile can no longer be described by the classical log law. Figure 12 shows mean velocity profiles from LES of the APG boundary layer approaching separation in inner scaling with the friction velocity U_τ and viscous length scale l^+. The scaled velocity profiles

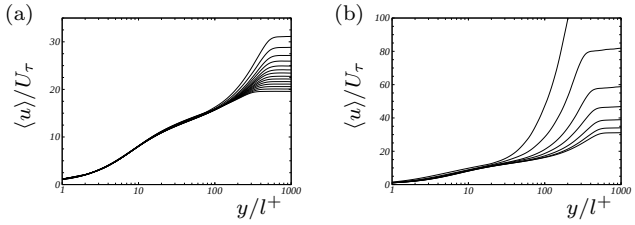

Figure 12: Classical inner scaling tested for mean velocity profiles of attached, decelerated boundary layer flow (a) with negligible backflow (b) approaching separation $0.1 \leq \chi \leq 0.5$.

do not collapse in the wake region and the classical log region is shortened.

Indinger (2005) found that also the level the log region shows an effect of the pressure gradient and reasoned that the failure of the classical inner scaling coincides with the very first occurrence of instantaneous reverse flow. The present LES reveals that inner scaling remains valid for substantial backflow and *intermittent transitory detachment* even for the shortened log layer. This mismatch between experiment and LES can be attributed to the Preston-tube measurement technique, used for determining l^+. The agreement of experiment and LES improves significantly, however, when the correlation of Fernholtz (1964) is used for determining the scaling parameters for the experimental velocity profiles. The inner scaling fails only close to the separation where the wall-friction velocity becomes smaller than Simpson's velocity scale based on the pressure gradient. It is worth to note that inner scaling can be improved locally at detachment when the pressure gradient is incorporated (Manhart et al., 2007).

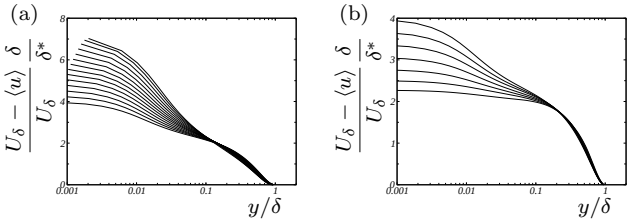

Figure 13: ZS scaling tested for mean velocity profiles of attached, decelerated boundary layer flow (a) with negligible backflow (b) approaching separation $0.1 \leq \chi \leq 0.5$.

Zagarola and Smits (1998) (ZS) propose a scaling based on the velocity scale $U_\delta \delta^*/\delta$. This scaling leads to much better collapse in the outer region that covers almost 90 percent of the boundary layer thickness, see Fig. 13. These findings are consistent with experimental results of Indinger et al. (2006).

CONCLUSIONS

We have presented a well resolved Large Eddy Simulation (LES) of turbulent boundary-layer separation. Investigated is an incompressible fully-turbulent flat-plate boundary layer subjected to a constant adverse pressure gradient (APG). The APG leads to a streamwise increasing fraction of back-flow events that eventually results in strong boundary-layer separation. Reynolds number and pressure-gradient parameters are adapted to measurements conducted by Indinger (2005) and Indinger et al. (2006, 2004) in a closed-circuit water tunnel. The computational results are discussed in detail and validated against experimental data. Conclusions are drawn con-

cerning the employed measurement technique and the scaling of the mean velocity profile of turbulent boundary-layer flow under non-equilibrium conditions in the vicinity of pressure-induced separation. Present LES and experimental results show consistently that the mean velocity profile can no longer be described by the classical log law. However, whereas Indinger found that the failure of inner scaling coincides with the very first occurrence of instantaneous reverse flow, the present numerical study reveals that inner scaling remains valid for intermittent transitory detachment. The same is found for the experimental data when Fernholtz's correlation technique is used for determining the scaling parameters of the experimental velocity profiles. Our results suggest that classical inner scaling is valid for $0 \leq y < 20l^+$ and the scaling of Zagarola and Smits (1998) is valid for $0.1\delta < y \leq \delta$.

ACKNOWLEDGMENTS

Dr. Indinger (TU München) is gratefully acknowledged for providing his experimental data and for many helpful discussions. This research is supported by the German Research Council (Deutsche Forschungsgemeinschaft - DFG) in the framework of the French-German research group FG507.

REFERENCES

Adams, N. A., S. Hickel, and S. Franz (2004). Implicit subgrid-scale modeling by adaptive deconvolution. *J. Comp. Phys. 200*, 412–431.

Dengel, P. and H. H. Fernholz (1990). An experimental investigation of an incompressible turbulent boundary layer in the vicinity of separation. *Journal of Fluid Mechanics 212*, 615–636.

Fernholtz, H.-H. (1964). Halbempirische gesetze zur berechnung turbulenter grenzschichten nach der methode der integralbedingungen. *Ingenieur-Archiv 33*(6), 384–395.

Garnier, E., M. Mossi, P. Sagaut, P. Comte, and M. Deville (1999). On the use of shock-capturing schemes for large-eddy simulation. *J. Comput. Phys. 153*, 273–311.

George, W. K. (2006). Recent advancements toward the understanding of turbulent boundary layers. *AIAA Journal 44*(11), 2435–2449.

Grinstein, F., L. Margolin, and W. Rider (Eds.) (2007). *Implicit Large Eddy Simulation: Computing Turbulent Flow Dynamics*. Cambridge, UK: Cambridge University Press.

Head, M. R. and V. V. Ram (1971). Improved presentation of preston tube calibration. *Aeronautical Quaterly 22*, 295–300.

Hickel, S. and N. A. Adams (2006). Efficient implementation of nonlinear deconvolution methods for implicit large-eddy simulation. In W. Nagel, W. Jäger, and M. Resch (Eds.), *High Performance Computing in Science and Engineering. Transactions of the High Performance Computing Center, Stuttgart (HLRS)*, pp. 293–306. Springer.

Hickel, S., N. A. Adams, and J. A. Domaradzki (2006). An adaptive local deconvolution method for implicit LES. *J. Comp. Phys. 213*, 413–436.

Hickel, S., N. A. Adams, and N. N. Mansour (2006). Implicit subgrid-scale modeling for large-eddy simulation of passive-scalar mixing. In *Proceedings of the 2006 Summer Program*, pp. 123–138. Center for Turbulence Research, Stanford University.

Hickel, S., T. Kempe, and N. A. Adams (2005). On implicit subgrid-scale modeling in wall-bounded flows. In *Proceedings of the EUROMECH Colloquium 469*, Dresden, Germany, pp. 36–37.

Hickel, S., T. Kempe, and N. A. Adams (2006). Implicit large-eddy simulation applied to turbulent channel flow with periodic constrictions. *Theoret. Comput. Fluid Dynamics*. (submitted).

Indinger, T. (2005). *Einfluss eines positiven Druckgradienten auf turbulente Grenzschichten an glatten und gerillten Oberflächen*. Ph. D. thesis, TU München.

Indinger, T., M. H. Buschmann, and M. Gad-el-Hak (2006). Mean-velocity profile of turbulent boundary layers approaching separation. *AIAA Journal 44*(11), 2465–2474.

Indinger, T., S. Hickel, and N. Adams (2004). 3d-measurements in an adverse-pressure-gradient turbulent boundary layer over smooth and ribbed surfaces. In *Proceedings of the 21st International Congress of Theoretical and Applied Mechanics (ICTAM)*, Warsaw, Poland.

Ludwieg, H. and W. Tillmann (1949). Untersuchungen über die Wandschubspannungen in turbulenten Reibungsschichten. *Ingenieur-Archiv 17*, 288–299.

Lund, T., X. Wu, and K. Squires (1998). Generation of turbulent inflow data for spatially-developing boundary layer simulations. *J. Comp. Phys. 140*, 233–258.

Maciel, Y., K.-S. Rossignol, and J. Lemay (2006). Self-similarity in the outer region of adverse-pressure-gradient turbulent boundary layers. *AIAA Journal 44*, 2450–2464.

Manhart, M., N. Peller, and C. Brun (2007). Near-wall scaling for turbulent boundary layers with adverse pressure gradient: A priori tests on DNS of channel flow with periodic hill constrictions and DNS of separating boundary layer. *Theoret. Comput. Fluid Dynamics*. (in press).

Morinishi, Y., T. Lund, O. Vasilyev, and P. Moin (1998). Fully conservative higher order finite difference schemes for incompressible flow. *J. Comput. Phys. 143*, 90–124.

Nagano, Y., T. Tsuji, and T. Houra (1998). Structure of turbulent boundary layer subjected to adverse pressure gradient. *International Journal of Heat and Fluid Flow 19*, 563–572.

Panton, R. L. (2005). Review of wall turbulence as described by composite expansions. *Applied Mechanics Reviews 58*(1), 1–36.

Patel, V. C. (1965). Calibration of the preston tube and limitations on its use in pressure gradient. *Journal of Fluid Mechanics 23*(part 1), 185–208.

Shu, C.-W. (1988). Total-variation-diminishing time discretizations. *SIAM J. Sci. Stat. Comput. 9*(6), 1073–1084.

Simpson, R. L. (1981). A review of some phenomena in turbulent flow separation. *J. Fluids Eng. 102*, 520–533.

Simpson, R. L. (1989). Turbulent boundary-layer separation. *Ann. Rev. Fluid Mech. 21*, 205–234.

Skåre, P. E. and P.-Å. Krogstad (1994). A turbulent equilibrium boundary layer near separation. *Journal of Fluid Mechanics 272*, 319–348.

Spalart, P. R. (1988). Direct simulation of a turbulent boundary layer up to $re_\theta = 1410$. *J. Fluid Mech. 187*, 61–98.

Zagarola, M. and A. Smits (1998). Mean-flow scaling in turbulent pipe flow. *J. Fluid Mech. 373*, 33–79.